Wu *et al. Chin. J. Mech. Eng.* (2019) 32:78
https://doi.org/10.1186/s10033-019-0392-0

Chinese Journal of Mechanical Engineering

ORIGINAL ARTICLE

Open Access

A Novel Pneumatic Soft Gripper with a Jointed Endoskeleton Structure

Zhaoping Wu*, Xiaoning Li and Zhonghua Guo

Abstract

In current research on soft grippers, pneumatically actuated soft grippers are generally fabricated using fully soft materials, which have the advantage of flexibility as well as the disadvantages of a small gripping force and slow response speed. To improve these characteristics, a novel pneumatic soft gripper with a jointed endoskeleton structure (E-Gripper) is developed, in which the muscle actuating function has been separated from the force bearing function. The soft action of an E-Gripper finger is performed by some air chambers surrounded by multilayer rubber embedded in the restraining fiber. The gripping force is borne and transferred by the rigid endoskeleton within the E-Gripper finger. Thus, the gripping force and action response speed can be increased while the flexibility is maintained. Through experiments, the bending angle of each finger segment, response time, and gripping force of the E-Gripper have been measured, which provides a basis for designing and controlling the soft gripper. The test results have shown that the maximum gripping force of the E-Gripper can be 35 N, which is three times greater than that of a fully soft gripper (FS-Gripper) of the same size. At the maximum charging pressure of 150 kPa, the response time is 1.123 s faster than that of the FS-Gripper. The research results indicate that the flexibility of a pneumatic soft gripper is not only maintained in the case of the E-Gripper, but its gripping force is also obviously increased, and the response time is reduced. The E-Gripper thus shows great potential for future development and applications.

Keywords: Soft gripper, Jointed endoskeleton, Gripping force

1 Introduction

In contrast to rigid grippers, soft grippers are suitable for gripping fragile and delicate objects having irregular shapes and sizes owing to their high flexibility [1–3]. Therefore, soft grippers have become the focus of current research. Several mature products have been applied into automatic product gripping and handling systems gradually [4–8].

Thus far, pneumatic actuation is one of the key research directions and applications for soft grippers. A fully soft starfish-like gripper has been developed by Harvard University and is fabricated from silicone rubber through photolithography and used for gripping objects of mass less than 100 g, such as eggs and guinea pigs, without damaging the object used in the bioscience research [9]. Several types of commercial soft grippers are manufactured by Soft Robotics Inc. (USA) and are used for gripping various fruit and light commodities in automatic production lines with a quick gripping response and a maximum gripping force of 500 g. A modularized soft gripper with embedded flexible curve sensors has been presented by Bianca S. Homberg at MIT. It was able to grip tools of mass less than 1 kg (gripping force of approximately 10 N) such as a tiny wrench or hammer [10]. A composite fluidic actuator with a circumferential fiber-reinforced structure has been studied at the Harvard Biodesign Lab. With the circumferential fiber-reinforced structure, radial expansion could be effectively reduced such that the rigidity and gripping force can be increased [11, 12].

Although current soft grippers have the advantages of flexibility and adaptability to irregular objects, they still have the general problem of an insufficient gripping force [13, 14]. Furthermore, the use of fully soft materials can result in some difficulty in the gripper operation. Soft materials lack rigidity, and this results in an insufficiency

*Correspondence: wuzhaoping008@sina.com
School of Mechanical Engineering, Nanjing University of Science and Technology, Nanjing 210094, China

Springer Open

© The Author(s) 2019. This article is distributed under the terms of the Creative Commons Attribution 4.0 International License (http://creativecommons.org/licenses/by/4.0/), which permits unrestricted use, distribution, and reproduction in any medium, provided you give appropriate credit to the original author(s) and the source, provide a link to the Creative Commons license, and indicate if changes were made.

of the gripping force; in contrast, radial expansion occurs in a soft actuator when it is pressurized, which decreases the output efficiency. Therefore, it is crucial to enhance the rigidity of a soft gripper as well as the gripping force and decrease the unnecessary deformations in the research.

To solve the above-mentioned problems, a novel pneumatic soft gripper with a jointed endoskeleton structure (E-Gripper for short) has been developed by the authors. The actuation and force bearing functions of the E-Gripper are delegated to separate parts of the gripper. Then, not only can the flexibility and adaptability of the soft material be maintained, but the rigidity and gripping force are also noticeably increased. With the new E-Gripper, the practical requirements of flexibility and a large gripping force can be preferably met. The specific structure and characteristics of the E-gripper are introduced in detail here.

2 Design of the Novel Structure

2.1 Inspiration

The merit of a pneumatic soft gripper is that it is flexible, but its shortcoming is that it has insufficient rigidity and gripping force. Through careful analysis, it can be determined that the action of the pneumatic soft gripper is performed by the bending deformation of the soft finger, which is driven by air pressure. This means that the soft materials are used as the action performer owing to their flexibility. However, the gravity force of a product is also borne and transferred by the soft material when gripping a product. The two functions of actuation and force bearing and transferring are performed by the same soft materials. As is well known that the rigidity of the soft materials is inferior to that of a rigid mechanical structure when bearing and transferring the force. Hence, there exists an inherent shortcoming of insufficient rigidity in fully soft grippers. If a soft material is used for performing flexible action under air pressure while the force bearing and transferring is performed by another rigid structure, the shortcomings of insufficient rigidity and gripping force may be overcome. This means that if the two above-mentioned functions, which were originally performed by the soft material part alone, could be separated and respectively performed by two parts, a novel and promising gripper could be developed. This is the inspiration for our research. After testing several design schemes, a structure of a soft gripper with a jointed endoskeleton is presented. In the overall structure, the actuator is encased in the fingers of the gripper, which are fabricated using silicon rubber, and the flexible deformation action of the silicon rubber is actuated by air pressure, while a rigid endoskeleton is embedded in the inner chamber of the soft finger. The embedded endoskeleton is joined by basic units that significantly increase the gripping force. Thus, both the flexibility and sufficient gripping force of the soft gripper are realized.

2.2 Structure of the E-Gripper

2.2.1 Structure of the Finger

A schematic of a single finger joint of the E-gripper is shown in Figure 1(a) and (b). The endoskeleton of the finger-joint is joined by endoskeleton units (1) and (2) at hinge (3). The left and right end faces of a chamber are formed by two endoskeleton units (1 and 2), on which holes (6) are opened as the air inlet and outlet. The outer part of the endoskeleton comprises poured silicon rubber, which is used for sealing the chamber and actuating the finger. The circumferential fiber windings (4) are wrapped in the silicon rubber (5) to restrain the radial deformation of the finger joint.

The bending deformation of the finger joint is shown in Figure 1(b). Owing to the restraint of the endoskeleton, when pressurized, the rotation action around the hinge axis would be generated with the stretching of the rubber layer in which there are no rigid parts. Thus, the finger joint is bent. The middle layer (4) is used for limiting the radial expansion such that the air energy can effectively be used for the bending action of the finger.

An entire soft finger with a jointed endoskeleton constituting multi-finger-joints is shown in Figure 2. When assembling the finger, a smooth taper shape is formed from the fingertip to the finger root with a size that increases gradually [15]. An endoskeleton consists of 16 basic units that are hinged to form 15 finger joints in

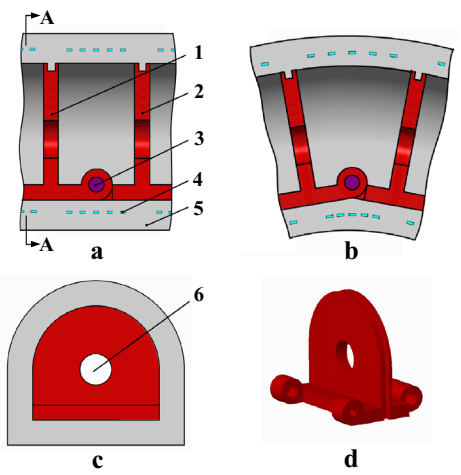

Figure 1 **a** Structure of a single finger joint; **b** Bending deformation of the finger joint during air charging; **c** A–A section view; **d** Three-dimensional view of an endoskeleton unit. 1. Endoskeleton unit 1; 2. Endoskeleton unit 2; 3. Hinge; 4. Fiber; 5. Silicon rubber; 6. Flow channel

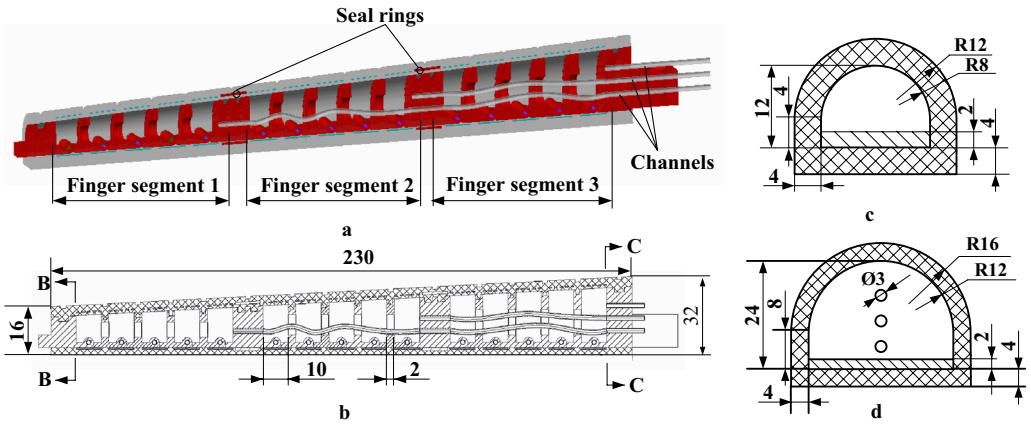

Figure 2 **a** Configuration of an entire soft finger; **b** Cross-section view; **c** B–B section view; **d** C–C section view (unit: mm)

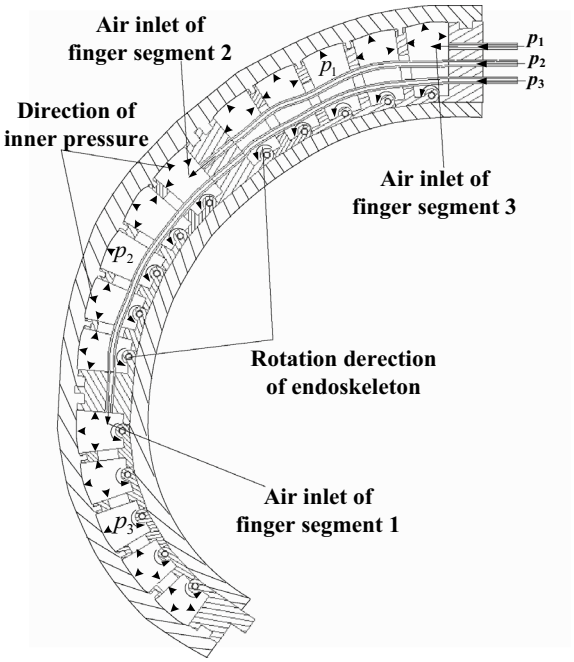

Figure 3 Schematic of bending of the soft finger

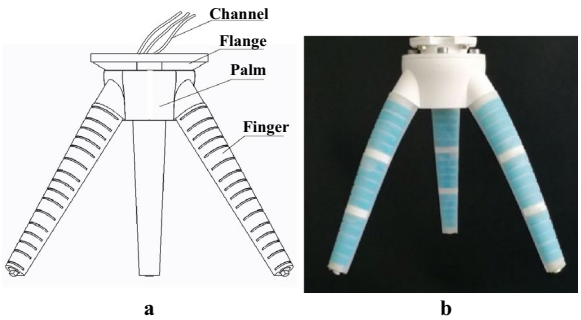

Figure 4 **a** Configuration of the E-Gripper; **b** Photograph of the E-Gripper

series. The finger joint can rotate from −45° to 180° at the hinge joints. To increase the operation efficiency and realize a greater number of postures, the entire finger is divided into three independent finger segments that can be independently pressurized using different air pressures to control the bending angle.

The working process is shown in Figure 3. Compressed air flows through the channels from the finger root to control three finger segments, and the air pressure is marked as p_1, p_2, and p_3, respectively, for the three finger segments. Bending deformation occurs at each finger joint under the air pressure and the tension of the silicon rubber. The expected output bending angle and torque could be obtained. The total bending angle of the finger is the sum of each finger joint's bending angle, and the total output torque of the finger is the sum of each finger joint's torque. The design comprising three finger segments can reduce the response time. When the fingers touch an object to form an enveloping grip, the applied force is transferred to the bottom of the palm through the endoskeleton. As compared with the FS-Gripper, the gripping ability can be obviously increased in this case.

2.2.2 Overall Gripper Structure

The assembled E-Gripper with three fingers is shown in Figure 4(a). The three fingers are evenly distributed on the circumference of the palm. The angle between the two adjacent fingers is 120°, and the angle between the axis of a finger and that of the palm is 35°. The palm is fabricated using a 3D printer and comprises flow channels passing to the fingers. The palm can be linked with a

robotic arm via a flange. A photograph of the E-Gripper is shown in Figure 4(b).

A finger with three segments and independent air charge are designed to obtain multi-degrees of freedom. If all the finger segments are respectively controlled, a greater number of postures could be realized in order to grip objects of different shapes and sizes, such as fruit and daily tools. When gripping tiny objects, the mode of fingertip gripping can be adopted. When gripping heavy objects, the mode of enveloping gripping with three charged segments can be adopted to increase the response speed.

2.3 Fabrication of the E-Gripper

2.3.1 Material Selection

Several materials are compositely used for fabricating the E-Gripper [16]. A light and rigid material should be used for the endoskeleton, such that fatigue damage owing to repeated bending can be avoided. PolyPlus^{TM} (a polylactic acid material produced by Polymaker) is then used for fabricating the endoskeleton using a 3D printer [10], which could meet the requirements. The actuating layer is fabricated using YZ FS6600 silicon rubber with a Shore-hardness of 10 A and an appropriate stretching property. Fibers are used for the embedded reinforced layer to limit radial deformation.

2.3.2 Fabrication Process

The E-Gripper is fabricated through modular components [17]. First, the basic units of an endoskeleton are linked at hinges (Figure 5(a)). Three air tubes are then embedded into the endoskeleton in order to control the different finger segments independently (Figure 5(b)). The soft actuating layer is casted in three steps. In the first step, one silicon rubber layer is glued around the endoskeleton according to the locating slot, while the seal ring is sealed at the intersection of the adjacent segments (Figure 5(c)). In the second step, the circumferential fiber is evenly wound on the surface (Figure 5(d)). In the last step, the outer silicon rubber layer is glued to form the finger (Figure 5(e)). Finally, the three fingers are connected to a palm to complete the fabrication of the E-Gripper (Figure 5(f)).

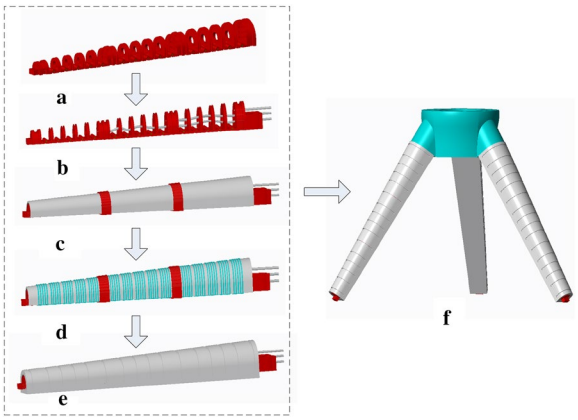

Figure 5 Fabrication progress of the E-Gripper. **a** The endoskeleton consists of several basic units. **b** Three tubes are embedded into the endoskeleton. **c** One silicon rubber layer is glued around the endoskeleton, and the seal rings are sealed. **d** Circumferential fiber is evenly wound on the surface. **e** A complete soft finger. **f** E-Gripper with three fingers

3 Mathematical Model

To determine the basic operating characteristics of the finger and gripper under air pressure, it is necessary to build develop a corresponding kinematic and mechanical model. Through the analysis of the mathematic model, the characteristics data such as the bending angle, response time, output torque, and gripping force under air pressure can be acquired to lay a foundation for the application of the gripper.

A soft finger can be treated as a system of n finger joints in series that share the same working principle. The mathematic model can be developed by taking one finger joint as an example. Then the entire finger is an N-linkage system [18, 19].

The soft finger with the jointed endoskeleton is a coupled pneumatic system, which consists of a large nonlinear deformation and multiple materials. It is difficult to develop an accurate mathematic model. For the convenience of theoretical analysis and obtaining a solution, there following simplifications are made:

(1) The air supply is assumed to be stable and constant.
(2) The radial deformation is negligible owing to the constraint of the circumferential fibers.
(3) The stretch of the silicon rubber is uniform.
(4) There is no friction between the adjacent joints.
(5) The axial length and bending angle of a single finger joint are small while the radius of curvature is large. Thus, the altitude difference of both ends is ignored, and the finger joint is simplified to a model with a constant radius of curvature.

3.1 Strain Energy Function Model of Material

The strain energy function of silicon rubber is used for deducing the stress and strain [20, 21]. There are many types of strain energy functions. The Yeoh model is applied in this paper owing to its ability in simulating large deformations [22].

For the general principle stress of a uniform strain, the true principle stress σ_i is

$$\sigma_i = 2\left(\lambda_i^2 \frac{\partial W}{\partial I_1} - \frac{1}{\lambda_i^2}\frac{\partial W}{\partial I_2}\right) + p_0, \quad i = 1, 2, 3, \tag{1}$$

where I_1 is the first principle invariant, I_2 is the second principle invariant, λ_i are the principle stretch ratios, p_0 is an arbitrary hydrostatic pressure, and

$$I_1 = \lambda_1^2 + \lambda_2^2 + \lambda_3^2, \tag{2}$$

$$I_2 = \lambda_1^2\lambda_2^2 + \lambda_2^2\lambda_3^2 + \lambda_3^2\lambda_1^2, \tag{3}$$

$$\lambda_1\lambda_2\lambda_3 = 1. \tag{4}$$

When p is pressurized, the base of the finger joint only bends around the axis of rotation without extension because of the limitation of the endoskeleton. The bending angle θ and radius of curvature correspond to each finger joint. The radial stretch ratio λ_2 is assumed to be 1 because of the fiber restrained layer. The axial stretch ratio λ_1 is determined as λ. The silicon rubber layer stretches uniformly. The circumferential stretch ratio λ_3 can be determined from the ratio of the stretched and initial thicknesses. Then according to Eq. (4), the following is obtained.

$$\lambda_1 = \lambda, \lambda_2 = 1, \lambda_3 = \frac{t}{t'} = \frac{1}{\lambda}, \tag{5}$$

where t is the initial thickness of the silicon rubber layer, and t' is the thickness of the silicon rubber layer after stretching.

From the Yeoh model, the strain energy function is expressed as

$$W = C_{10}(I_1 - 3) + C_{20}(I_2 - 3)^2 + C_{30}(I_1 - 3)^3, \tag{6}$$

where C_{10}, C_{20}, and C_{30} are the coefficients of the primary, quadratic, and cubic terms, respectively, which can be obtained through calibration tests.

A vanishing stress is assumed in the radial direction ($\sigma_3 = 0$), and the circumferential σ_2 is much smaller than the axial true principle stress σ_1. Then σ_1 is considered to be the only nonzero principle stress, which is defined as σ. From Eqs. (2)–(3), the following is obtained:

$$\begin{aligned}\sigma = {} & 2(\lambda^2 - 1)\left[C_{10} + 3C_{30}\left(\lambda^2 + \frac{1}{\lambda^2} - 2\right)^2\right] \\ & - 4C_{20}\left(\frac{1}{\lambda^2} - 1\right)\left(\lambda^2 + \frac{1}{\lambda^2} - 2\right).\end{aligned} \tag{7}$$

3.2 Static Model of Bending

A static model of a single finger joint is derived to obtain the bending angle. The schematic of the model is shown in Figure 6. As described in Figure 1, the two endoskeleton units are simplified to obtain ones with nondeformable boundaries, which can only rotate around the axle of the joint, while the silicon rubber extends when pressurized.

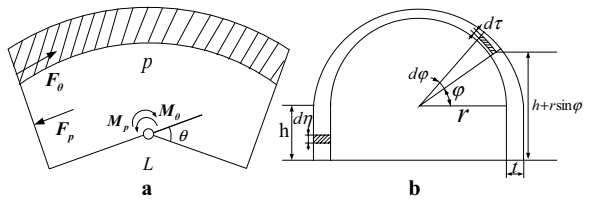

Figure 6 **a** Static model of the finger joint during bending; **b** Cross-sectional view of the finger joint

When bending deformation occurs under internal air pressure, there exists forces such as the tensile stress of the silicon rubber F_θ and the acting force F_p between the endoskeleton units. Accordingly, there is a balance among the torques around the axis of rotation. The torque generated by the internal air pressure acts as the driving moment M_p, the torque generated by the stretching stress is the resistance moment M_θ, and the torque of the acting force is 0.

The torque equilibrium can then be obtained as

$$M_p = M_\theta. \tag{8}$$

The driving moment M_p generated by the internal air pressure can be written as

$$M_p = \int_0^h p2r\eta \mathrm{d}\eta + \int_0^{\frac{\pi}{2}} p2r\cos\left(\arccos\frac{\varphi}{r}\right) r\mathrm{d}\varphi. \tag{9}$$

Next, the resistance moment M_θ can be integrated in two parts.

From 0 to the height of h,

$$\lambda_\eta = \frac{L + \eta\theta}{L}. \tag{10}$$

From height h to the top,

$$\lambda_{\tau,\varphi} = \frac{L + h\theta + \sin\varphi r\theta}{L}, \tag{11}$$

where L is the initial axial length of the finger joint model.

Moreover, by introducing the strain energy function Yeoh model Eq. (7), the resistance moment can be expressed as

$$\begin{aligned}M_\theta = {} & 2\int_0^h \sigma_\eta t'\eta \mathrm{d}\eta \\ & + 2\int_0^{\frac{\pi}{2}}\int_0^{t'} \sigma_{t,\varphi}((r+\tau)^2\sin\varphi + h(r+\tau))\mathrm{d}\tau\mathrm{d}\varphi.\end{aligned} \tag{12}$$

A relationship between the input air pressure and the output angle can then be described using the simultaneous Eqs. (5)–(12):

$$\theta = \delta(r, h, L, t, p). \tag{13}$$

By introducing the geometrical parameters (r, h, L, t) of the different finger joints, the bending angle of each finger joint can be obtained. Through testing, it is found that the deformation of each finger joint has little influence on the others. Thus, for each finger joint, only the driving moment M_p and resistance moment M_θ are considered.

A finger segment consists of five finger joints. Owing to the complete independence of each finger joint, a continuum robot system is built and each finger joint is regarded as a robot joint. The D–H method is used to develop the coordinate system shown in Figure 7. XOY is the fixed reference system, and one coordinate system is fixed at each finger joint [23].

The bending angle of a finger segment is

$$\theta_j = \sum_{i=1}^{5} \theta_i, \tag{14}$$

where θ_i is the angle of the ith finger joint, and θ_j is the angle of the jth finger segment.

The displacement transformation matrix of two adjacent coordinate systems is expressed as

$$T_i^{i-1} = \begin{bmatrix} c_i & -s_i & 0 & L_i c_i \\ s_i & c_i & 0 & L_i s_i \\ 0 & 0 & 1 & 0 \\ 0 & 0 & 0 & 1 \end{bmatrix}, \tag{15}$$

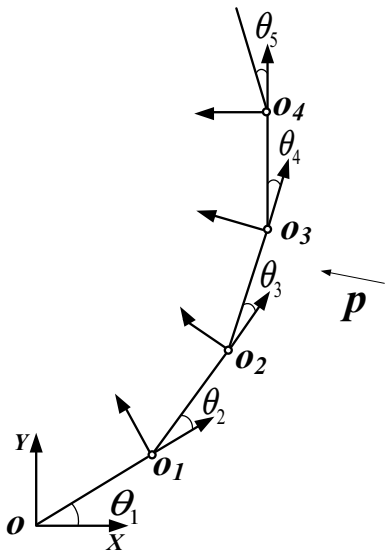

Figure 7 Cartesian coordinate system of a single finger segment

where $c_i = \cos\theta_i$; $s_i = \sin\theta_i$; and L_i is the length of the ith finger joint.

Moreover, an arbitrary coordinate system relative to the fixed reference system XOY is

$$T_i^0 = \begin{bmatrix} c_{1,i} & -s_{1,i} & 0 & L_i c_{1,i} + L_{i-1} c_{1,i-1} + \cdots + L_1 c_1 \\ s_{1,i} & c_{1,i} & 0 & L_i s_{1,i} + L_{i-1} s_{1,i-1} + \cdots + L_1 s_1 \\ 0 & 0 & 1 & 0 \\ 0 & 0 & 0 & 1 \end{bmatrix}, \tag{16}$$

where $\sin_{1,i} = \sin(\theta_1 + \theta_2 + \cdots + \theta_i)$; $\cos_{1,i} = \cos(\theta_1 + \theta_2 + \cdots + \theta_i)$.

3.3 Dynamic Model of Bending

A dynamic model is developed to acquire the dynamic response characteristics under pressurization. Finger segment j (Figure 2) is considered as an example for analysis. The finger segment is simplified to its equivalent in the form of one chamber. The values of the equivalent geometrical parameters (r_j, h_j, L_j, t_j) of the chamber are obtained, and the corresponding rotational inertia J_j is calculated. The dynamical equation is

$$\sum M_j = J_j \frac{\mathrm{d}^2\theta_j}{\mathrm{d}t^2} + C\frac{\mathrm{d}\theta_j}{\mathrm{d}t}, \quad (j = 1, 2, 3), \tag{17}$$

where J_j is the rotational inertia of the equivalent chamber, $J_1 = 0.025\ \mathrm{kg \cdot m^2}$, $J_2 = 0.035\ \mathrm{kg \cdot m^2}$, $J_3 = 0.048\ \mathrm{kg \cdot m^2}$; C is the viscous damping coefficient of the equivalent chamber, $C = 0.1\ \mathrm{N\,m \cdot s/rad}$; and $\sum M_j$ is the resultant moment of the equivalent chamber, N·m.

As mentioned above, the acting force between the joints has a slight influence on the bending of the chamber. Only the driving moment M_{jp} and resistance moment $M_{j\theta}$ are considered; then

$$\sum M_j = M_{jp} - M_{j\theta}. \tag{18}$$

On introducing the parameters (r_j, h_j, L_j, t_j), M_{jp} and $M_{j\theta}$ can be solved using Eqs. (9)–(12).

Considering that the silicon rubber is a material with a low thermal conductivity, while the duration of the actual charging and discharging process is short thus resulting in insufficient time to facilitate the heat exchange of the air between the chamber and surroundings. The thermodynamics process can be treated as a reversible adiabatic process (isentropic process). Consequently, the working process can be regarded as an insulation system with variable mass and volume [24, 25].

According to the principle of conservation of energy, the conversion equation of pressure in the chamber is expressed as

$$\frac{\mathrm{d}p}{\mathrm{d}t} = \frac{\kappa R T_s Q_{ms}}{V_j} - \frac{\kappa p}{V_j}\frac{\mathrm{d}V_j}{\mathrm{d}t}, \tag{19}$$

where κ is the polytropic exponent of the air.

The relation between the volume of the chamber and the bending angle is

$$V_j = \frac{4r_j^3 + 3\pi h_j r_j^2 + 6h_j^2 r_j}{6}\theta_j + \frac{4h_j r_j + \pi r_j^2}{2}L_j, \quad (20)$$

where p is the pressure in the chamber, Pa; θ_j is the bending angle of the chamber, rad; κ is the adiabatic exponent of air, $\kappa = 1.4$; $R$is the gas constant, $R = 287.1$ J(kg · k); T_s is the temperature of the air source, i.e., room temperature of 298.5 K; Q_{ms} is the influx mass flow rate, kg/s; and V_j is the volume of the chamber.

Moreover, the mass flow equations can be expressed as

$$Q_{ms} = c_c A_s p_s \sqrt{\frac{2\kappa}{RT_s(\kappa-1)}}\varphi\left(\frac{p}{p_s}\right), \quad (21)$$

$$\varphi\left(\frac{p}{p_s}\right) = \begin{cases} 0.2588, & \sigma = \dfrac{p}{p_s} \le 0.528, \\ \sqrt{\sigma^{\frac{2}{\kappa}} - \sigma^{\frac{\kappa+1}{\kappa}}}, & \sigma = \dfrac{p}{p_s} > 0.528, \end{cases} \quad (22)$$

where c_c is the air shrinkage coefficient, $c_c = 1.5$; A_s is the area of the air inlet; p_s is the upstream pressure.

The dynamic bending model of the soft gripper can be obtained according to Eqs. (17)–(22). Owing to the complexity of the model, it is difficult to obtain an analytical solution. Therefore, the Runge–Kutta method in MATLAB is used for solving the multi-stage differential equations.

3.4 Mechanical Model of Enveloping Gripping

For different objects, different gripping modes can be used. One of the modes is the enveloping gripping with which the fingers can finely fit an object surface to increase the contacting area and friction force, as well as the gripping force [26, 27]. The enveloping gripping is analyzed and modeled as follows.

The output torque of a finger is first modeled. As mentioned above, the bending angle and output torque are only related to the actuation torque and drag torque of the silicon rubber. Let us assume that the finger has just touched the object at the bending angle θ and with pressure p. With Δp added, the angle and tensile stress are invariant, and the output torque $M_{\Delta p}$ can be expressed as

$$M_{\Delta p} = J_{\Delta p}^{\mathrm{T}} \Delta p, \quad (23)$$

where $J_{\Delta p}^{\mathrm{T}}$ can be expressed according to Eq. (9).

A simplified mechanical model of the enveloping gripping can be derived by referring to Figure 8. The bearing force of each finger is equal to the normal pressure and friction force of the gripped object. The resultant force of the three symmetric fingers is equal to the gravity of the object. Hence, only one of the fingers should be analyzed. For one finger, the external torque M_e generated by the normal pressure and friction force is

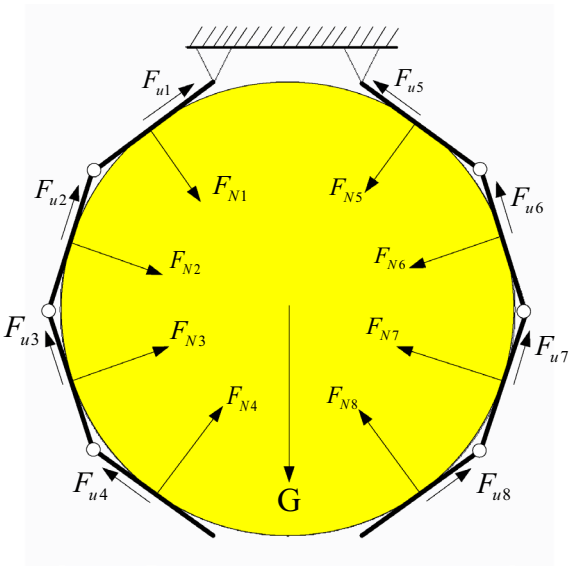

Figure 8 Force analysis of the enveloping gripping

$$M_e = M_N + M_f, \quad (24)$$

where M_N is the external torque generated by all the positive forces, and M_f is the external torque generated by all the friction forces.

The torque generated by the normal pressure and friction force can be derived according to the number and location of the actual contact points [28]. That is, $M_N = J_N^{\mathrm{T}} F_N$, and $M_f = J_f^{\mathrm{T}} F_f$.

According to the torque equilibrium, the output torque $M_{\Delta p}$ is then balanced with the external torque M_e, and the torque equation is

$$J_{\Delta p}^{\mathrm{T}} \Delta p = J_N^{\mathrm{T}} F_N + J_f^{\mathrm{T}} F_f. \quad (25)$$

The normal force F_N at the contact point is an active force and can be measured. The friction force F_f is a passive force, which is uncontrollable and can only be evaluated through the increment of pressure and positive force indirectly [29]. These analysis results can aid in designing the gripper for gripping the object and in controlling the E-Gripper.

4 Testing for Characteristics and Gripping

An experimental platform was developed to test the working characteristics and gripping performance of the E-Gripper. Corresponding experimental schemes

were designed to measure the bending angle, response time, and gripping force of the enveloping gripping when pressurized.

4.1 Bending Angle

An experiment scheme (Figure 9) was designed to measure the bending angle based on data acquisition controller (Simulink software). The bending angle can be controlled via three independent proportional pressure valves, and using an industrial personal computer, 15 points were marked along the axis of the joint on the finger surface. The soft finger was set up horizontally with a fixed root and free tip. A high-definition television (HDTV) camera was used to capture photographs of the finger in real time. A photograph of the finger was captured every 5 kPa. The coordinates of the marked points were extracted and analyzed to obtain the bending angle of the three finger segments. The relationship between the input pressure and bending angle was then determined.

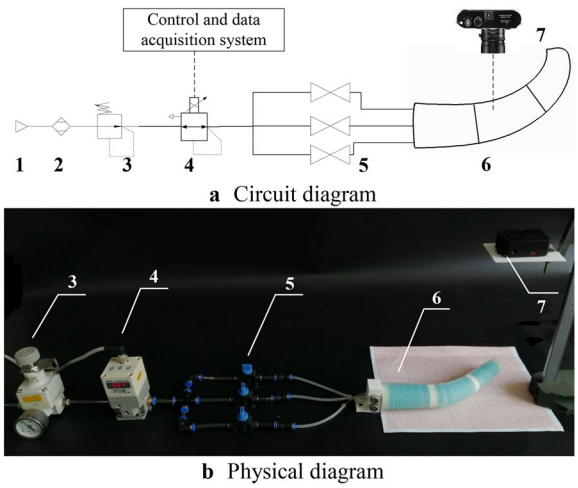

Figure 9 Schematic of bending angle testing system. 1. Air source; 2. Dryer; 3. Reducing valve; 4. Proportional pressure valve; 5. Shut-off valve; 6. Finger; 7. HDTV camera

The strain–stress curve of the silicon rubber PS6600-10A was measured via a tensile test [29]. The coefficients of the Yeoh model were obtained ($C_{10}=4.94\times10^{-2}$, $C_{20}=-.75\times10^{-3}$, and $C_{30}=4.41\times10^{-2}$). The bending angle of each chamber was calculated through MATLAB software according to the mathematic model. The curves of the bending angle of the fingertip are shown in Figure 10. The variation trend of the theoretical data is consistent with that of the experimental ones. When the input pressure is below 100 kPa, the theoretical curves coincide well with the experimental one. However, when the input pressure is greater than 100 kPa, the theoretical curves are above the experimental curves. This is because the silicon rubber presents a high nonlinearity at a large deformation.

To quantitatively compare the theoretical values with the experimental ones, the relative difference is defined as

$$d_p = \frac{|\theta_A - \theta_E|}{\theta_A} \times 100\%, \tag{26}$$

where d_p, θ_A, and θ_E are the relative difference, theoretical bending angle, and experimental bending angle, respectively.

The values of the relative difference are summarized in Table 1. It is found that the maximum difference is less than 9% with a maximum working pressure of 150 kPa. This indicates that the mathematic model of the bending angle is valid.

4.2 Response Time

In industrial applications, a shorter response time is expected, and thus, the working cycle could be shortened. However, a normal pneumatic soft gripper often has a long gripping response time because of the rubber's deformation delay and the flow resistance. Therefore, a structure of three finger segments is designed, which

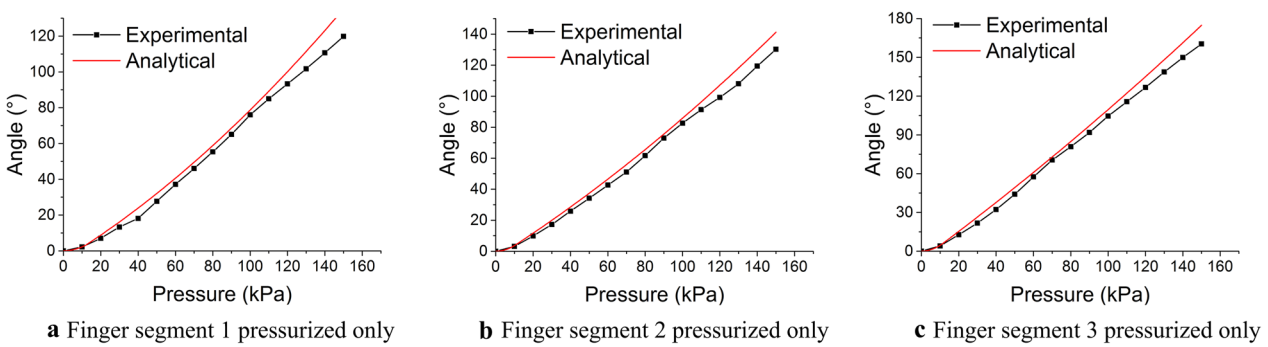

Figure 10 Bending angles of the fingertip under the pressurization of different finger segments

Table 1 Relative difference of bending angles of each finger segment (%)

Pressure (kPa)	30	60	90	120	150
Finger segment 1	3.6	4.64	7.70	6.33	6.62
Finger segment 2	3.91	4.93	8.98	8.14	7.69
Finger segment 3	6.16	7.94	6.27	7.45	8.09

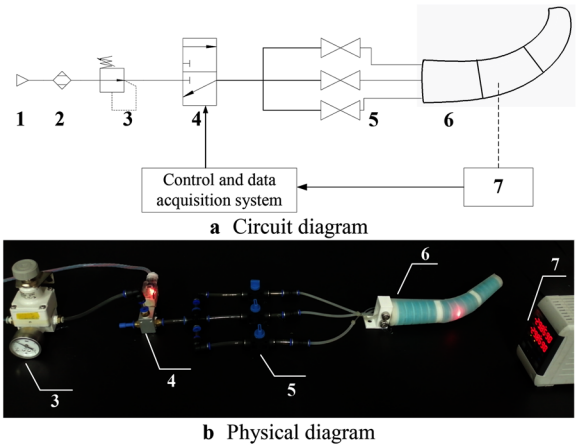

Figure 11 Schematic of response time testing system. 1. Air source; 2. Dryer; 3. Reducing valve; 4. Solenoid directional valve; 5. Shut-off valve; 6. Finger; 7. Laser displacement sensor

can be simultaneously charged to decrease the gripping response time. For this purpose, the corresponding measurements were obtained.

At first, the response time of each finger segment was measured. A solenoid directional valve with a high response speed was used to control the air charging and discharging. A laser displacement sensor was considered to follow the motion of the finger segment to obtain the response time. The open response time of the directional valve can be ignored because it is much shorter than that of the finger. The testing schematic is shown in Figure 11.

Table 2 Response time of two grippers (ms)

Pressure (kPa)	30	60	90	120	150
E-Gripper	66	138	192	277	321
FS-Gripper	253	576	795	1215	1444

The curves of the theoretical calculation and measured response time of each finger segment are shown in Figure 12. The theoretical curve is essentially fit with the measured one. Although the theoretical values are a little larger than measured ones, but the relative error is still small. It can be seen that with the smallest volume of chamber at the tip the first finger segment has the shortest response time while with the largest volume at the root the third finger segment has the longest response time.

The response time data of the E-Gripper with three parallel finger segments and the FS-Gripper of the same size with a single segment are listed in Table 2. Under different working pressures, the response time of the E-Gripper is between 66 ms and 321 ms, while that of the FS-Gripper is between 253 ms and 1.4 s. The response time of the E-Gripper is 187 ms faster than that of the FS-gripper at 30 kPa and is 1123 ms faster than that of the FS-gripper at 150 kPa. This indicates that the response time of the E-Gripper is much faster than that of the FS-Gripper, especially under high pressures.

4.3 Gripping Force and Object Gripping Demo

4.3.1 Gripping Force Measurement

Gripping force is an important parameter of a gripper. The new E-Gripper is embedded with the endoskeleton, which could increase the gripping force while maintaining flexibility. In order to compare the gripping force of

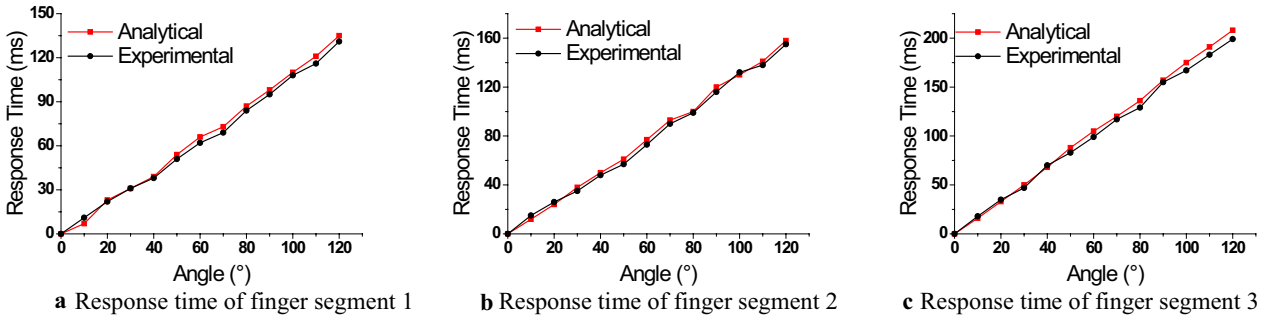

Figure 12 Response time of each finger segment

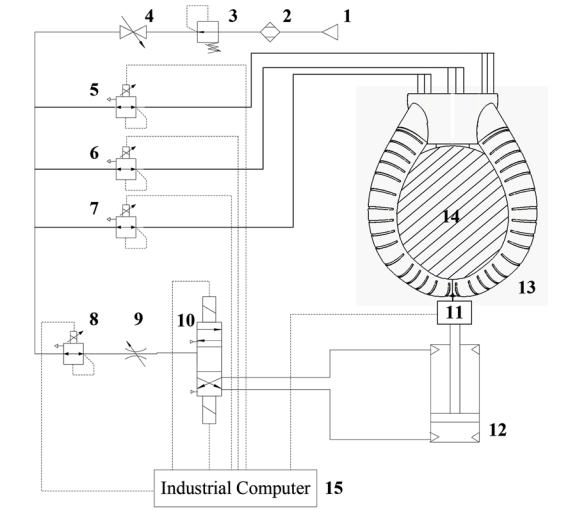

a Circuit diagram

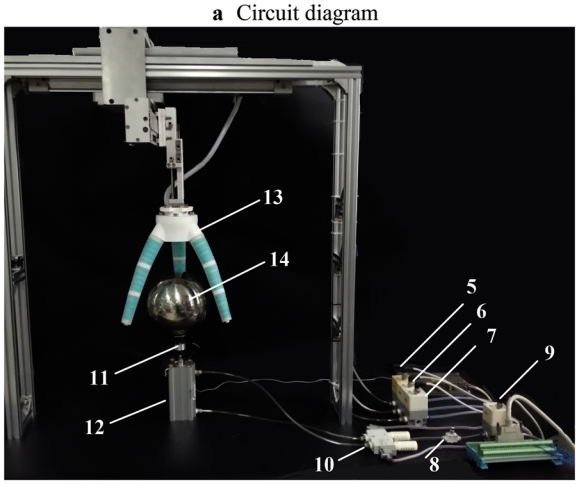

b Physical diagram

Figure 13 Gripping force testing circuit. 1. Air source; 2. Dryer; 3. Reducing valve; 4. Shut-off valve; 5, 6, 7, 8. Proportional pressure valve; 9. Throttle valve; 10. Solenoid directional valve; 11. Tension sensor; 12. Cylinder; 13. E-Gripper; 14. Sphere; 15. Computer

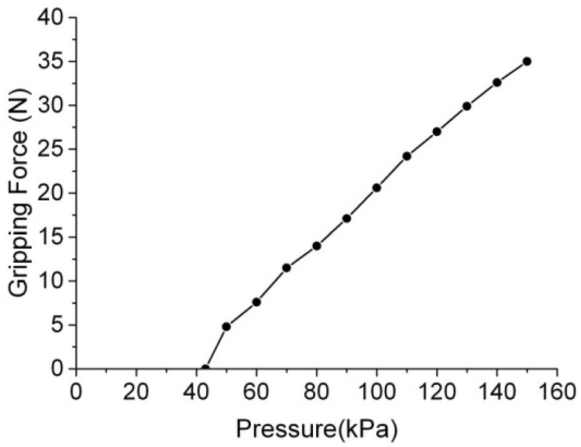

Figure 14 Largest gripping force of the E-Gripper under different working pressures

the FS-Grippers with that of the E-grippers, a measuring system was developed as shown in Figure 13.

An air cylinder was used as the quantified loading device, and an aluminous sphere of 180-mm diameter was used as the reference object. One end of a tension sensor JHBM-10 kg was connected on the bottom of the sphere, while the other end was connected with the cylinder. Four proportional pressure valves were used to control the gripping movement and the loading force of the cylinder. At the beginning of the test, the tension sensor and sphere rose to the marked workspace driven by the cylinder. Three finger segments were inflated using the same working pressure from 0 kPa to 150 kPa through proportional pressure valves. A downward-moving loop of the cylinder was switched every 10 kPa. Meanwhile, a first-order signal was sent to the proportional pressure valve 10 to increase the pressure slowly until the sphere separated from the gripper and moved downward. The data of the tension sensor were acquired by computer in real time.

The variation of the gripping force with the working pressure is shown in Figure 14. It can be observed that the enveloping grip of the sphere is accomplished at approximately 43 kPa, where there is a minimum gripping force. Furthermore, the gripping force has a quasi-linear relation with the input pressure, which provides the theoretical foundation for the control of practical gripping. From Figure 14, it can also be observed that the largest gripping force can be 35 N, i.e., the mass of the gripped object is approximately 3.5 kg at the maximum working pressure of 150 kPa. The gripping force of the E-Gripper is 3.5 times greater than that of the FS-Gripper mentioned in Ref. [10].

We inferred that, by means of the endoskeleton, the maximum gripping force of the E-Gripper is significantly increased because the gripping force is directly transferred to the palm through the endoskeleton instead of the soft actuator.

4.3.2 Object Gripping Demonstration

The E-Gripper can be used for gripping objects of different shapes and sizes. Photographs of the E-Gripper when gripping several objects are shown in Figure 15. An aluminous sphere, a cloth doll, and a glass bulb are chosen as the heavy, soft, and fragile objects, respectively, for the gripping demonstration. The experimental results showed that the heavy sphere, soft doll, and fragile bulb can be effectively gripped by the E-Gripper, which

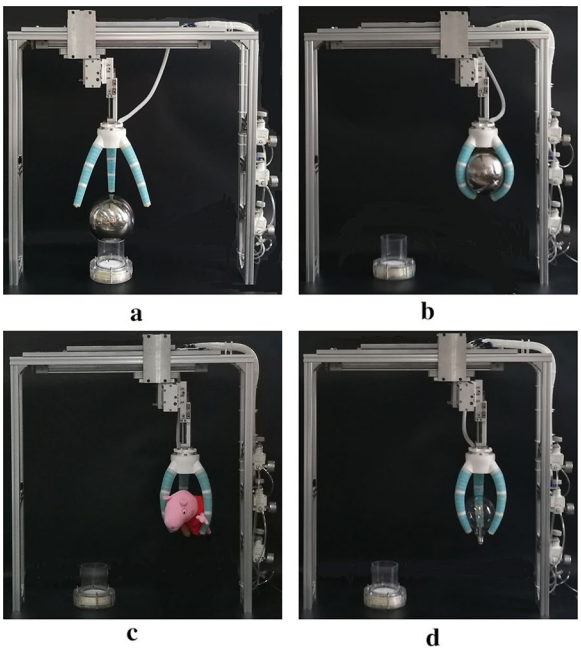

Figure 15 **a** Ready for gripping; **b** Gripping an aluminous sphere; **c** Gripping a cloth doll; **d** Gripping a glass bulb

indicates that both high flexibility and a sufficient gripping force are obtained. The E-Gripper can be qualified in practical operation.

5 Conclusions

To solve the problem of the mutual restriction between the flexibility and gripping force in a pneumatic gripper, an innovative design of the structure of a soft gripper with separate functioning parts has been developed. The achievements of this research are summarized as follows:

(1) A novel pneumatic soft gripper with a jointed endoskeleton structure (E-Gripper) is developed, in which, the actuation and force bearing functions can be separated. The bending action of a finger of the E-Gripper is performed by the soft rubber with an embedded radial-restrained fiber through pneumatic actuation, while the gripping force is borne and transferred by means of the jointed endoskeleton. Thus, the inherent limitation of the FS-Gripper whereby the actuating and force bearing functions are undertaken by the same component can be overcome by the new E-Gripper. The gripping force can then be increased, and a high flexibility can be maintained.

(2) The modeling and analysis of the kinematic and mechanical characteristics of a finger of the gripper are performed. The relation between the bending angle θ_i and input pressure p and that between the output torque and positive pressure as well as the friction force are acquired. From the theoretical analysis and the measured pressure-angle displacement curves, it can be observed that the gripping force has a quasi-linear relation with the input pressure within the rated working pressure (approximately 150 kPa), and the gripping force also has a quasi-linear relation with the input pressure after touching the gripped object. The variation laws have provided a valuable foundation for the design and operation of the E-Gripper. Moreover, the structure of three finger segments with parallel air supply has increased the response speed and provided more flexible controlling modes for gripping objects of various shapes and sizes.

(3) Experiments indicate that the maximum gripping force of the E-Gripper is up to 35 N with the rated working pressure of 150 kPa, which is 3.5 times greater than the gripping force of 10 N of the FS-Gripper that is reported in the extant literature. Moreover, the response time of the E-Gripper is 1.123 s faster than that of the FS-Gripper of the same size at a pressure of 150 kPa, which aids in shortening the working cycle and increasing the efficiency in practical operation.

The research results indicate that the design of the structure of the novel pneumatic soft gripper with a jointed endoskeleton is successful and the E-Gripper has great potential for future development and application.

Authors' Contributions

ZW was in charge of the whole trial; ZW wrote the manuscript; XL and ZG assisted with sampling and laboratory analyses. All authors read and approved the final manuscript.

Authors' Information

Zhaoping Wu, born in 1988, is currently a PhD candidate at *School of Mechanical Engineering, Nanjing University of Science and Technology, China.* He received his bachelor degree from *Nanjing University of Science and Technology, China*, in 2011. His research interests include pneumatic control technology, soft actuator design and control.

Xiaoning Li, born in 1957, is currently a professor at *School of Mechanical Engineering, Nanjing University of Science and Technology, China.* He received his PhD degree from *Harbin Institute of Technology, Harbin, China,* in 1989. His research interests include modeling, simulation, and control for advanced manufacturing systems, and pneumatic control technology, etc.

Zhonghua Guo, born in 1983, is currently a master student supervisor at *School of Mechanical Engineering, Nanjing University of Science and Technology, China.* She received her PhD degree from *Nanjing University of Science and Technology, China*, in 2012. Her research interests include pneumatic components, pneumatic vacuum system, soft actuator design, etc.

Competing Interests

The authors declare that they have no competing interests.

Funding
Supported by National Natural Science Foundation of China (Grant No. 51305202) and Jiangsu Provincial Natural Science Foundation of China (Grant No. BK20130764).

Received: 23 August 2018 Revised: 21 April 2019 Accepted: 4 September 2019
Published online: 23 September 2019

References

[1] C Majidi. Soft robotics: a perspective—current trends and prospects for the future. *Soft Robotics*, 2014, 1(1): 5-11.
[2] R Deimel, O Brock. A compliant hand based on a novel pneumatic actuator. *IEEE International Conference on Robotics and Automation*, Karlsruhe, Germany, May 6-10, 2013: 2047-2053.
[3] R Deimel, O Brock. *A novel type of compliant and underactuated robotic hand for dexterous grasping*. Thousand Oaks: Sage Publications, Inc., 2016.
[4] M E Giannaccini, I Georgilas, I Horsfield, et al. A variable compliance, soft gripper. *Autonomous Robots*, 2014, 36(1-2): 93-107.
[5] S Wakimoto, K Ogura, K Suzumori, et al. Miniature soft hand with curling rubber pneumatic actuators. *IEEE International Conference on Robotics and Automation*, Kobe, Japan, May 12-17, 2009: 556-561.
[6] Z Wang Z, D S Chathuranga, S Hirai. 3D printed soft gripper for automatic lunch box packing. *IEEE International Conference on Robotics and Biomimetics*, Qingdao, China, December, 2017: 503-508.
[7] J R Amend, E Brown, N Rodenberg, et al. A positive pressure universal gripper based on the jamming of granular material. *IEEE Transactions on Robotics*, 2012, 28(2): 341-350.
[8] T Matsuno, Z Wang, S Hirai. Grasping state estimation of printable soft gripper using electro-conductive yarn. *Robotics & Biomimetics,* 2017, 4(1): 13.
[9] F Ilievski F, A D Mazzeo, R F Shepherd, et al. Soft robotics for chemists. *Angewandte Chemie International Edition*, 2011, 50(8): 1890-5.
[10] B S Homberg, R K Katzschmann, M R Dogar, et al. Haptic identification of objects using a modular soft robotic gripper. *IEEE/RSJ International Conference on Intelligent Robots and Systems*, Hamburg, Germany, September 28-October 2, 2015: 1698-1705.
[11] P Polygerinos, K C Galloway, S Sanan, et al. EMG controlled soft robotic glove for assistance during activities of daily living. *IEEE International Conference on Rehabilitation Robotics*, Singapore, August 11-14, 2015: 55-60.
[12] P Polygerinos, Z Wang, J T B Overvelde, et al. Modeling of Soft Fiber-Reinforced Bending Actuators. *IEEE Transactions on Robotics*, 2015, 31(3): 778-789.
[13] C T Loh, H Tsukagoshi. Pneumatic Big-hand gripper with slip-in tip aimed for the transfer support of the human body. *IEEE International Conference on Robotics and Automation*, Hong Kong, China, May 31 - June 7, 2014: 475-481.
[14] R V Martinez, J L Branch, C R Fish, et al. Robotic tentacles with three-dimensional mobility based on flexible elastomers. *Advanced Materials*, 2013, 25(2): 153-153.
[15] L Margheri, C Laschi, B Mazzolai. Soft robotic arm inspired by the octopus: I. From biological functions to artificial requirements. *Bioinspiration & Biomimetics*, 2012, 7(2): 025004.
[16] D Rus, M T Tolley. Design, fabrication and control of soft robots. *Nature*, 2015, 521(7553): 467.
[17] F J Chen, S Dirven, W L Xu, et al. Soft actuator mimicking human esophageal peristalsis for a swallowing robot. *IEEE/ASME Transactions on Mechatronics*, 2014, 19(4): 1300-1308.
[18] X Liu, Y Wang, D Geng, et al. Mechanical characteristics analysis on PAM with elongation and torsion. *International Conference on Mechatronic Science, Electric Engineering and Computer*, Jilin, China, Aug 19-22, 2011: 613-616.
[19] Z Wang, S Hirai. Soft gripper dynamics using a line-segment model with an optimization-based parameter identification method. *IEEE Robotics & Automation Letters*, 2017, 2(2): 624-631.
[20] Y Kamel, B Hocine. A new hyper-elastic model for predicting multi-axial behaviour of rubber-like materials: formulation and computational aspects. *Mechanics of Time-Dependent Material*, 2017(7): 1-20.
[21] B Kim, S B Lee, S Cho, et al. A comparison among Neo-Hookean model, Mooney-Rivlin model, and Ogden model for chloroprene rubber. *International Journal of Precision Engineering & Manufacturing*, 2012, 13(5): 759-764.
[22] J L Huang, G J Xie, Z W Liu. Finite element analysis of super-elastic rubber materials based on the Mooney-Rivlin and Yeoh model. *China Rubber/Plastics Technology and Equipment*, 2008, 34(12): 22-26. (in Chinese)
[23] Y L Xiong. *Fundamentals of robotics.* Wuhan: Huazhong University of Science & Technology Press, 1996. (in Chinese)
[24] J F Li. *Pneumatic transmission system dynamics*.Guangzhou: South China University of Technology Press, 1991. (in Chinese)
[25] A D Marchese, R Tedrake, D Rus. Dynamics and trajectory optimization for a soft spatial fluidic elastomer manipulator. *IEEE International Conference on Robotics and Automation,* Seattle, USA, May 26-30, 2015: 2528-2535.
[26] J C Trinkle. *The mechanics and planning of enveloping grasp*. USA: University of Pennsylvania, 1987.
[27] K Harada, M Kaneko. Enveloping grasp for multiple objects. *Proc. of IEEE Int. Conf. on Robotics & Automation*, 2010, 16(6): 860-867.
[28] S Qian, L Zhang, Q Yang, et al. Research on output force of flexible pneumatic bending joint. *International Conference on Control, Automation, Robotics and Vision*, Hanoi, Vietnam, December 17-20, 2009: 144-148.
[29] S H Li, H M Jia, et al. Theory and testing method of hyperelastic material constitutive model. *China Elastomerics,* 2011, 21(1): 58-64. (in Chinese)

Submit your manuscript to a SpringerOpen journal and benefit from:

► Convenient online submission
► Rigorous peer review
► Open access: articles freely available online
► High visibility within the field
► Retaining the copyright to your article

Submit your next manuscript at ► springeropen.com